Soil aggregate geometry: Measurements and morphology

F. San José Martínez , F.J. Muñoz Ortega , F.J. Caniego Monreal , A.N. Kravchenko , W. Wang

Keywords:
Soil aggregates
X-ray computed tomography
Mathematical morphology
Morphological operations
Minkowski functionals
Morphological functions
Conventional tillage
Native succession vegetation treatment

A B S T R A C T

Aggregates provide physical microenvironments for microorganisms, the vital actors of soil systems, and thus play a major role as both, an arena and a product of soil carbon stabilization and dynamics. The surface of an aggregate is what enables exchange of the materials and air and water fluxes between aggregate exterior and interior regions. We made use of 3D images from X-ray CT of aggregates and mathematical morphology to provide an exhaustive quantitative description of soil aggregate morphology that includes both intra-aggregate pore space structure and aggregate surface features. First, the evolution of Minkowski functionals (i.e. volume, boundary surface, curvature and connectivity) for successive dilations of the solid part of aggregates was investigated to quantify its 3D geometrical features. Second, the inner pore space was considered as the object of interest. We devised procedures (a) to define the ends of the accessible pores that are connected to the aggregate surface and (b) to separate accessible and inaccessible porosity. Geometrical Minkowski functionals of the intra-aggregate pore space provide the exhaustive characterization of the inner structure of the aggregates. Aggregates collected from two different soil treatments were analyzed to explore the utility of these morphological tools in capturing the impact on their morphology of two different soil managements, i.e. conventional tillage management, and native succession vegetation treatment. The quantitative tools of mathematical morphology distinguished differences in patterns of aggregate structure associated to the different soil managements.

1. Introduction

Soil aggregates are key elements of soil structure that play a major role in several soil processes including the accumulation and protection of soil organic matter, the optimization of soil water and air regimes, and the storage and availability of plant nutrients (von Lützow et al., 2006). Intra-aggregate properties strongly affect all these functions. It has been shown that gradients of a number of soil characteristics exist inside soil aggregates. Among them are gradients in oxygen concentrations of the soil air (Sexstone et al., 1985), gradients in concentrations of a variety of elements, including Ca, Mg, K, Na, Mn, K, Al, and Fe (Jasinska et al., 2006; Santos et al., 1997), and gradients in organic matter compositions (Ellerbrock and Gerke, 2004; Urbanek et al., 2007). These differences in intra-aggregate characteristics in turn influence activities and compositions of soil microbial communities (Blackwood et al., 2006; Jasinska et al., 2006). Aggregates are of particular importance for processes of soil carbon sequestration (Chenu and Plante, 2006; Six et al., 2000). It has been shown that intra-aggregate characteristics, such as size-distributions of intra-aggregate pores, can be directly related to the amount of C stored inside the aggregate (Ananyeva et al., 2013).

The influence of long-term management differences manifests itself not only on the overall soil aggregation but also on the intra-aggregate characteristics. The use of advanced X-ray 3D imaging techniques has greatly increased our ability to explore intra-aggregate features in intact aggregates and resulted in a large number of studies that demonstrated that tillage, land use and fertilization regime can have a major effect on intra-aggregate pore characteristics (Kravchenko et al., 2011; Peth et al., 2008; Wang et al., 2012; Zhou et al., 2013; Zucca et al., 2013).

In particular, it is known that converting the land that has been long under intensive agricultural management back to its natural vegetation will often result in a number of changes in soil characteristics, including increase in soil organic matter and increase in numbers and stabilities of soil macro-aggregates (e.g., De Gryze et al., 2004; Grandy and Robertson, 2007). These changes result from combined influences of a removal of soil disturbance by tillage and of an increase in diversity and duration of the plant biomass inputs to soil. We have observed marked effects on intra-aggregate characteristics of macro-aggregates in the soil that was abandoned from agriculture and was under native vegetation succession for the past 18 years. Such aggregates had greater heterogeneity in intra-aggregate pore distributions as compared with the aggregates from conventional agriculture (Kravchenko et al., 2011).

Another characteristic of the soil macro-aggregates that can have a substantial effect on their functioning is the properties of the aggregate surfaces. The surface of an aggregate enables exchange of the materials and air and water fluxes between the interior and exterior layers of aggregates. Its characteristics along with numbers and properties of soil pore opening at the aggregate surfaces influence the accessibility

of aggregate interiors to microbes, and thus can influence the ability of aggregates to protect soil carbon. It is likely that long-term differences in land use and management can affect the characteristics of the aggregate surfaces, however, to our best knowledge there have been no studies that specifically addressed this question.

A number of studies have been conducted to explore aggregate structure and investigate soil functioning. Image analysis and conventional mathematical measurements were used to quantify that structure. Whalley et al. (2005) studied the structural differences of adjacent soil to roots and bulk soil with image analysis of thin sections of aggregates. De Gryze et al. (2006) evaluated porosity and pore size distribution of the voids of aggregates as well as its mass fractal dimension with 2D sections of CT images. They were interested in the changes of pore structure during decomposition of fresh residue. Microbial micro-habit structure was investigated by Nunan et al. (2006) by combining synchrotron-based CT, image analysis and geostatistics of soil aggregates. Also fractal geometry have been use to quantify that structure. Young and Crawford (1991) devised a simple method to estimate fractal dimension with the mass and size of soil aggregates. Giménez et al. (2002) studied the changes of this fractal dimension for intact and eroded soil aggregates of cultivated and wooded soils. Image analysis of thin section of soil aggregates was used to estimate porosity and fractal dimension by Papadopoulos et al. (2006). They wanted to quantify the effects of contrasting crop in the development of soil structure. CT technology was used by Gibson et al. (2006) to compare fractal analytical methods on 2D and 3D. Chung Chun et al. (2008) used image analysis of thin section of soil aggregates to examine pore structure inside aggregates with lacunarity and entropy functions. More recently, Kravchenko et al. (2011) explored the effect of long-term differences in tillage and land use on intra-aggregate pore heterogeneity with fractal techniques.

In this work, a quantitative description of the internal geometrical characteristics as volume and connectivity of intra-aggregate pore space and of the external features as area and shape of aggregates' surface with the unified framework that provides mathematical morphology (Serra, 1982) through morphological tools known as the Minkowski functionals is proposed. Mathematical morphology offers a plethora of mathematical techniques to analyze and parameterize the geometry of different features of soil structure. These techniques belong to well established mathematical fields as integral geometry (Santaló, 1976), stochastic geometry (Matheron, 1975) or digital topology and geometry (Klette and Rosenfeld, 2004). They make available a sound mathematical background that guides the process from image acquisition and analysis to the generation of synthetic models of soil structure (Arns et al., 2004) to investigate key features of flow and transport phenomena in soil (Lehmann, 2005; Mecke and Arns, 2005).

In the sixties, the need for analyzing spatial data from geology led to Matheron and his colleagues at the Paris School of Mines at Fontainebleau (France) to the introduction and development of computer technologies and mathematical techniques that now are known as mathematical morphology (Serra, 1982). Dullien and collaborators (see Dullien, 1992 and the references therein) made use of these techniques to investigate the relationship between soil pore structure and fluid flow phenomena. At that time they mostly used stereology to gain three-dimensional information from two-dimensional images obtained by image analysis of soil sections (Horgan, 1998; Moran et al., 1989a, 1989b; Vogel and Kretzschmar, 1996; Vogel et al., 2005).

X-ray computed tomography (CT) provides a direct procedure to use three-dimensional information to quantify geometrical features of soil pore space (Lehmann et al., 2006). In the last few decades mathematical morphology has been successfully used to analyze different characteristics of the rich three-dimensional geometrical information gained through X-ray CT (Banhart, 2008). Among the tools of mathematical morphology, Minkowski functionals are particularly worthy of consideration since they provide computationally efficient means to measure four fundamental geometrical properties of three dimensional geometrical objects such as soil aggregates. Their prominence relies on the mathematical fact (Santaló, 1976) that any other geometrical measurement that meets some self-evident and natural geometrical restrictions is a linear combination of these Minkowski functionals. Moreover, they represent four very familiar geometrical attributes: the volume, the boundary surface, the mean boundary surface curvature and the connectivity of the pore space. These functionals are powerful tools to quantitatively describe 3D geometry. Mecke (1998) and Roth et al. (2005) made use of Minkowski functions based on threshold variation of Minkowski functionals to characterize two-dimensional porous structures. Also, two-dimensional porous structures were investigated by Mecke (2002) and Vogel et al. (2005) with Minkowski functions based on dilations and erosions. Arns et al. (2002, 2004) considered the evolution of Minkowski functionals with dilations and erosions to characterize 3D images of Fontainebleau sandstone.

This paper is organized as follows. The building blocks of mathematical morphology are introduced in Section 2. Firstly, we introduce the morphological operations of dilation, erosion, opening and closing. Then, we described Minkowski functionals and the morphological functions. Technical details are presented in Appendix A. Section 3 is devoted to the description of the data set, the computation of Minkowski functionals and morphological functions, and the partition of aggregate pore space into accessible and inaccessible porosity. Technical details of that partition are given in Appendix B. Section 4 presents the results and discussion in the light of the main goals of this work, which are: (i) to provide a comprehensive quantitative description of soil aggregate structure through the morphological analysis of 3D CT images that includes both, aggregate surface features and intra-aggregate pore space structure, and (ii) to explore the ability of these techniques to detect changes in soil characteristics associated with long-term differences in land use and soil management.

2. Theory: morphological analysis

Morphological analysis mimics other scientific procedures and in some instances can be seen as a two-step process. To illustrate this point, let us consider the procedure to determine particle size distributions by sieving. This technique first generates a series of subsets of primary mineral particles corresponding to each sieve size; then, these subsets are weighted. In morphological analysis, first, geometrical transformations are applied to the object of interest in an image and then, measurements are carried out. When the granulometry – i.e., the grain size distribution – of an image of grains of different sizes shall be determined, successive morphological operations are performed on the image. These operations consist in the elimination of grains smaller than a certain size with a suitable morphological transformation. Each one of these operations is followed by the measurement of the area for 2D images or the volume for 3D images, of the grains left (Serra, 1982). Fig. 1 illustrates this procedure in a CT image of packed sand particles. In the following paragraphs, the basic morphological operations of dilation and erosion will be presented. Other two fundamental operations are opening and closing, that are defined in terms of dilations and erosions, will be introduced latter. Finally the notions of Minkowski functionals and morphological functions will be described. Additional details of these mathematical tools may be found in Appendix A.

2.1. Transformations: morphological operations

Grains or pore space in a 3D CT image will be idealized as 3D shapes (i.e. sets of points, K, in a three-dimensional space). The original object of interest, K, will be transformed by spheres of radius r centered at point x, B_x, – *structuring elements* – that will be called *balls*. The *dilation* by balls of radius r defines a new object $\delta_{rB}(K)$. Roughly speaking it is like a layer of thickness r is added to K. It is the union of all balls of radius r centered at points of object (Fig. 2). The *erosion* by the same type of

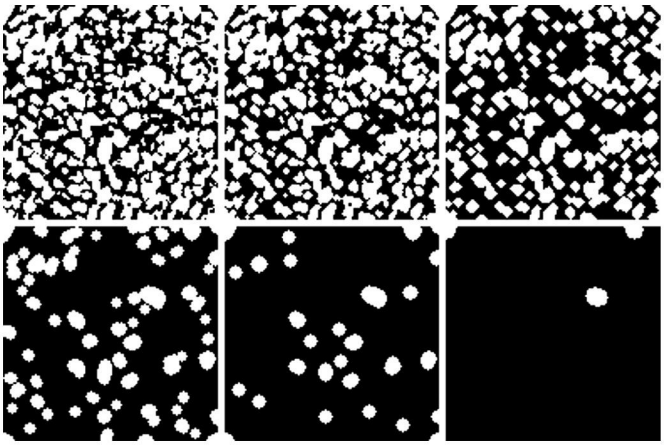

Fig. 1. Granulometric analysis of a section of a CT image of packed of sand particles by successive morphological operations.

balls produces an object $\varepsilon_{rB}(K)$ that is obtained as a layer of thickness r is removed from K (Fig. 2). For 2D objects, if one considers an object K as the only element of a picture surrounded by a frame, the erosion is equivalent to the dilation of the object that remains inside the frame when K is cut out from the framed picture. The object that remains inside the frame is called the *complementary* of K with respect to the framed picture and it is denoted by K^c. When K is a 3D object one will have a framed cube instead of a framed picture and K^c will be the remaining 3D object once K is cut out from the framed cube.

If dilation is performed after erosion the new morphological operation is an opening. When the order is reversed the new operation is a closing. If dilations expand the components of an image and erosion shrinks them, openings generally smooth out the contour of an object, break narrow isthmuses and eliminate thin protrusions while closings also tend to smooth out sections of contours but, opposite to openings, they generally fuse narrow breaks and long thin gulfs, eliminate small holes and fill gaps in the contour (Serra, 1982). Opening is the morphological operation that provides the granulometry of an image (Vogel, 2002). A more intuitive description of these operations can be gained through the complementary property stated above. Opening and closing are complementary operations of each other as erosions and dilations are. Let us consider, in the plane, the structuring element rB (a disk of radius r) as a rolling disk inside K, then the boundary of $O_{rB}(K)$ is determined by the points in the disk that reach the farthest into the boundary of K as rB is rolled around the inside of this boundary (Fig. 2). Closing has a similar geometric interpretation, except that now the disk rB is rolled on the outside of the boundary (Gonzalez and Woods, 2008) (Fig. 2).

One important feature of the closing operation for this investigation is the ability to remove the porosity of objects by applying successive closings with balls of increasing radius. In fact, in the limit, as the radius of the balls tends to infinity, a new one object called the convex hull is obtained (Serra, 1982). An object K is convex when it contains any point of the segment that joints two points in K (Fig. 3). The convex hull of an object K is the smallest convex set that contains K. Then, applying a certain amount of closings with successive balls of increasing radius, till disappearing of porosity, will provide a new object that, in general, is smaller than the convex hull of K. The volume of this new object can be considered as the volume of the smallest region that contains K and is connected (i.e. any two points of the region can be connected by a curve contained in the same region) and solid (with no porosity). Latter, this idea will be exploited in order to provide a realistic notion of the volume of an aggregate and that of its accessible porosity (i.e. pores connected to the exterior surface of the aggregate).

2.2. Measurements: Minkowski functionals

There are four Minkowski functionals in the space (see the Appendix for a more detailed description of Minkowski functionals), $W_i^{(3)}$, $i = 0, 1, 2, 3$. First and second Minkowski functionals have a simple geometrical interpretation. They correspond to volume, $V(K)$, and boundary surface area, $S(K)$, respectively.

When the boundary surface of a three-dimensional object is smooth, the third functional, the surface integral of the mean curvature, $M(K)$, might be an indicator of the surface boundary shape (Osher and Mücklich, 2000). Points on the boundary surface of an object with positive curvatures are located on convex parts (protrusions) while points with negative curvatures belong to concave parts (hollows). Hence, the mean curvature of convex points will be positive while it will be negative for concave points. Taking into account that the surface integral of the mean curvature over a certain boundary region of K may be interpreted as the average of the mean curvature over this surface

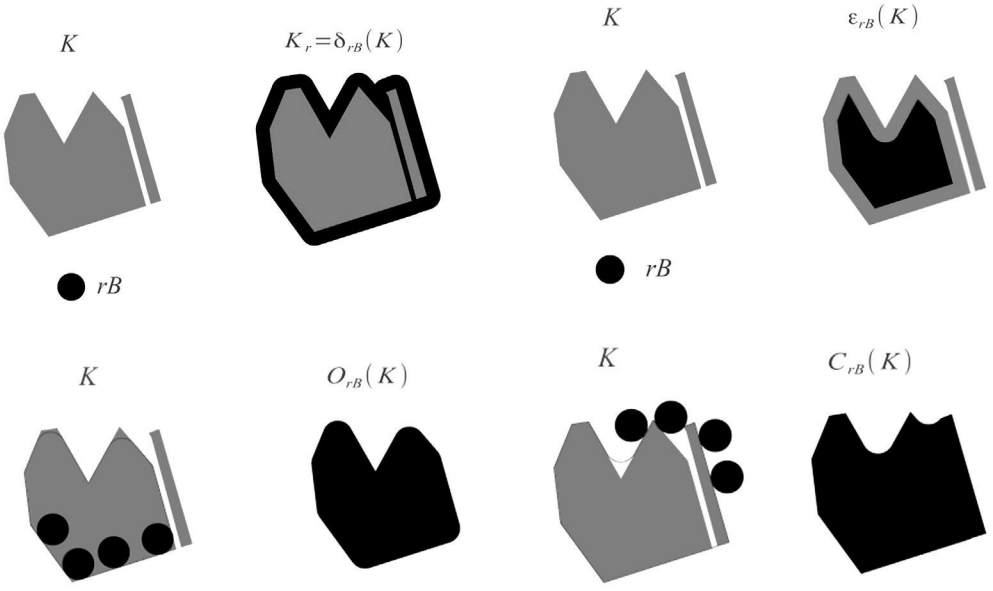

Fig. 2. 1: Dilation of K by the structuring element rB or the r-parallel body of K. 2: Erosion of K by the structuring element rB. 3: Opening (upper) and closing of an object (lower) of K by the structuring element rB.

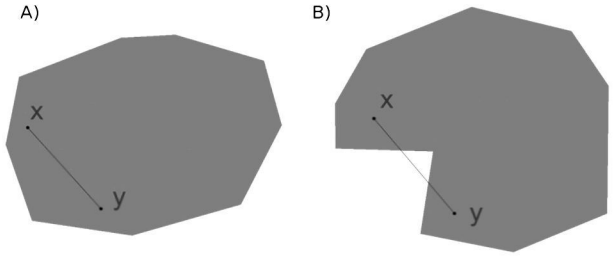

Fig. 3. A convex set (left) and a non-convex set (right).

region, the third functional, $M(K)$, should be positive for convex parts of the boundary surface while it should be negative for concave parts.

The fourth and last Minkowski functional is the Euler–Poincaré characteristic, $\chi(K)$, of the object up to a factor; this factor is the volume of the ball of radius one: $W_3^{(3)}(K) = (4\pi/3)\chi(K)$. When the object of interest K corresponds to the pore space P, the Euler–Poincaré characteristic $\chi(P)$ is an index of the topology of the pore phase because it does not refer to any metrics, and it quantifies pore connectivity (Vogel and Kretzschmar, 1996). In the plane, Euler–Poincaré can be computed subtracting the number of holes of the object, $H(K)$, from the number of connected components, $CC(K)$ (Mecke, 1998):

$$\chi(K) = CC(K) - H(K). \tag{1}$$

In this context, a connected component of an object is a connected part of this object: a part of the object where any two points can be connected by a curve completely contained in that part of the object (i.e. any point can be "visited" from any other of this part without stepping outside of it). Then, a disk has Euler–Poincaré characteristic equal to one, a punctured disk, zero, a disk punctured twice, minus one and so on. If the object is just the union of n separated grains on an image, Euler–Poincaré characteristic equals n. Similar definitions and relations hold for 3D shapes though distinction between two kinds of "holes" must be made. In this case, the Euler–Poincaré characteristic can be computed as the sum of the number of connected components, $CC(K)$, and the number of cavities of the object, $C(K)$, subtracted by the number of tunnels, $T(K)$ (Mecke, 1998):

$$\chi(K) = CC(K) - T(K) + C(K). \tag{2}$$

Cavities are holes completely surrounded by the object, while tunnels are holes through the object which connect the object with its exterior (i.e. the exterior is the complementary of the object with respect to the binary image). If the object is just a separate union of n grains of an image, Euler–Poincaré characteristic equals n. Then, a solid ball has Euler–Poincaré characteristic equal to one, a ball with a cavity on it, two, a ball with two cavities, three, and so on. But, if the ball has a tunnel that goes through it, the Euler–Poincaré characteristic is zero, two tunnels give a Euler–Poincaré characteristic equal to minus one, and so on. When the object of interest K is the soil matrix, their tunnels and cavities represent the accessible and the inaccessible soil porosity, respectively. For an aggregate that has only one connected component a positive Euler–Poincaré characteristic indicates preeminence, in number, of cavities or inaccessible porosity, while a negative characteristic is related to the preeminence in number of tunnels or accessible porosity.

Another important feature of Minkowski functionals is that they are easy to compute (Michielsen and De Raedt, 2001). Taking into account the C-additivity property (see the Appendix) and the fact that digital images are sets of cubes (or voxels), their computation reduces to the computation of the Minkowski functionals on cubes and their intersections (vertices, edges and faces) (Likos et al., 1995).

2.3. Morphological functions: describing objects by functions

Mathematical morphology offers a powerful description of objects in terms of functions that synthesizes the abovementioned two step view of morphological techniques. These functions generalize the process that provides particle size distributions by morphological analysis of soil images (Serra, 1982; Soille, 2002; Vogel, 2002).

Consider a 3D binary image of an object K, the object of interest. Let $\delta_{rB}(K)$ be, as before, the dilation of K by balls of radius r. Then, consider any Minkowski functional, say M, and the function

$$f(r) = M(\delta_{rB}(K)). \tag{3}$$

This family of functions built over the Minkowski functionals provides a way to investigate the morphology of the pore space K as it is dilated with balls of increasing radius r. When K is convex these functions do not carry extra information about the object because there are Steiner formulae (see the Appendix) for each Minkowski functional similar to the Steiner formula for the area or the volume (Osher and Mücklich, 2000). But there are no similar expressions for non-convex objects.

3. Materials and methods

3.1. Sampling and image acquisition

Soil aggregate samples were collected from the Long Term Ecological Research Site (LTER), Kellogg Biological Station located in southwest Michigan. For details on site description, experimental design and research protocols see http://lter.kbs.msu.edu (Kellogg Biological Station, 2011). The two LTER treatments that were sampled are (1) a conventional tillage management (chisel-plowed) with corn–soybean–wheat rotation and conventional chemical inputs (LTER-TM), and (2) native succession vegetation treatment, abandoned from agricultural management after spring plowing in 1989 (LTER-NS). Comprehensive description of sampling procedures, aggregate characteristics, image acquisition and pre-processing of this date set have been published elsewhere (Kravchenko et al., 2011; Wang et al., 2012).

3.2. Image segmentation

Each 3D image consisted of 520 slices with 696 × 696 pixels per slice. The voxel size was 14.6 μm. After pre-processing, the grayscale values in the images ranged from 0 (black) to 255 (white) corresponding to low and high X-ray absorptions, respectively. ImageJ (http://rsb.info.nih.gov/ij/index.html), a public domain Java image processing program inspired by NIH Image developed at the National Institutes of Health, was used to generate binary images of soil aggregates using the modes method (Sonka et al., 1998). In this procedure the histogram is iteratively smoothed until there are only two local maxima. Then, the threshold is chosen at the midpoint between these local maxima. The segmentation process provides a way to separate the object of interest from the background, in this case the solid material part from the pore space of the aggregate. This process produces binary images when a threshold is selected and any voxel with a grayscale value related with higher absorption of X-ray than the selected threshold is considered as part of the solid material and set to 1 (black), while any voxel with a grayscale value that correspond to lower absorption than the selected threshold is considered as part of the pore space of the aggregates or the background and set to 0 (white). When the object of interest is the pore space, value 1 is associated with the voxels of the voids of the aggregate. We selected a global method as we focused primarily on the analysis of geometrical features (Iassonov et al., 2009).

3.3. Computing Minkowski functionals

Minkowski functionals were computed on digitalized binary images of soil aggregates. Geometrical measurements were obtained with a computer code program developed by Michielsen and De Raedt (2001). For the sake of clarity, let us illustrate the procedure in two dimensions. In 2D, images have pixels that geometrically are squares with a characteristic length corresponding to the pixel size. Thus, the object of interest K is the finite union of black squares (compact and convex object) in a binary digital image. Each square may be considered as if it was made up of the four points of their four vertices, the four open segments of their four edges and the open square (i.e. the interior of the square). Therefore, the square of each pixel is the union of nine disjoint sets: four points, four open segments and the interior of the square. As a consequence, only the Minkowski functionals of three different types of sets (i.e. a point, an open segment and an open square) are needed and then C-additivity (see the Appendix) extended to the union of an arbitrary amount of sets can be used to compute the Minkowski functionals of the object of interest. If n_s is the number of open squares of the object, n_e the number of open edges and n_v the number of vertices of the pixels of the object of interest counted once, it is easy to verify that (Michielsen and De Raedt, 2001)

$$A(K) = n_s, L(K) = -4n_s + 2n_e \text{ and } \chi(K) = n_s - n_e + n_v. \quad (4)$$

A similar argument shows that (Michielsen and De Raedt, 2001) for 3D objects

$$V(K) = n_c,\ S(K) = -6n_c + 2n_f,\ \pi^{-1}M(K) = 3n_c - 2n_f + n_e \text{ and } \chi(K) = -n_c + n_f - n_e + n_v. \quad (5)$$

In this expression n_c is the number of (open) cubes and n_f is the number of faces (open squares) of the voxels of the object K counted once. As stated before, the Euler–Poincaré characteristic describes the connectivity of the object. In order to council this global topological point of view with the local computational procedure in terms of numbers of cubes, faces, edges and vertices, just mentioned above, it is necessary to define when two pixels and when two voxels are connected (Michielsen and De Raedt, 2001). In the plane two black pixels will be connected when they have an edge or a vertex in common. In the three-dimensional space two black voxels are connected when they have a face, an edge or a vertex in common.

3.4. Morphological functions with dilations

In our case, the set of voxels K, that represents the object of interest, corresponds to the solid part of one particular aggregate. This mathematical object will be dilated with balls of radius r. A series of objects $\delta_{rB}(K)$ will be obtained and the Minkowski functionals of the dilated objects $\delta_{rB}(K)$ will be evaluated. These operations will provide four functions that assign a number to each chosen value of the radius r of the ball B_r that dilates the object K; they are $\varphi_i(r) = \mathscr{F}_i(\delta_{rB}(K))$. Here $\mathscr{F}_i$ stands for volume when $i = 0$, boundary surface when $i = 1$, mean curvature for $i = 2$ and Euler–Poincaré characteristic when $i = 3$. These functions will display the evolution of these geometrical quantities when the radius of the ball that dilates the aggregate changes.

3.5. Partition of pore volume into accessible and inaccessible porosity

In order to have a more detailed information of aggregate porosity it is imperative to know what is the amount of pore space volume that goes to *tunnels*, that is, pores connected to exterior surface of the aggregate or what will be referred to as accessible porosity; and what is the amount of pore space volume that goes to *cavities*, that is, pores not connected to exterior surface of the aggregate or what will be considered as inaccessible porosity. It is important to answer the following question, how pore volume splits between accessible porosity and inaccessible porosity? This question leads us to the problem of the definition of the volume of a tunnel based on sound geometrical principles. Where are the ends of a tunnel? However, this is not an easy question to answer. Let us consider, for instance, a tunnel with trumpet-like ends. Then, a procedure to determine ends of tunnels is needed, but also a mean to distinguish tunnels from cavities in order to estimate the amount of the volume of accessible and inaccessible porosity of an aggregate and quantify the geometry of aggregate porosity.

So as to separate aggregate porosity between inaccessible and accessible porosity, different "parts" of the aggregate image should be identified. In loose terms, the image is made up of two "parts", the solid part of the aggregate, this is the object of interest (K), and the background, the rest of the image (K^c). While the object of interest cannot be decomposed into pieces, in this case, the background is made up of several parts. Any two points or voxels of K can be joined by a path of voxels that belongs to the solid part of the aggregate, K. So, as indicated before, K has only one connected component. But, the background, K^c, has several connected components. Each cavity of the inaccessible porosity is a connected component and the rest of the background forms another connected component. The later connected component is the set of voxels of the accessible porosity of the aggregate and its "exterior". It is clear that any two voxels of this set of voxels may be joined by a path of voxels that belongs to the same set.

In the continuum model, where objects are sets of points of the three-dimensional space, the notion of path or curve does not need any further explanation. In the discrete model, where objects are made up of voxels, the notion of path is related to the notion of what may be considered as a neighbor voxel to a given one or, equivalently, what should be understood by adjacent voxels. A path of voxels is made up of neighbor voxels. Consistency problems force to define different adjacencies for the object of an image and for its background (Kong and Rosenfeld, 1989). As it was stated before, when voxels belong to the object of interest, two voxels are neighbor when they share a face or an edge or a vertex (Michielsen and De Raedt, 2001). Then a voxel of the object of interest has twenty six neighboring voxels. When voxels belong to the background, they have six neighbors, any of the six voxels that share a face with it.

Our procedure to split aggregate porosity goes as follows. The connected components of the image are labeled (Rosenfeld and Pfaltz, 1966) and the inaccessible porosity is considered as part of the solid part of the aggregate. This is done by turning into back voxels the voxels of the inaccessible. Hence, from the original object K a new object K_T, whose voxels are the solid part of the aggregates plus the voxels of the cavities, is generated. This new object has no inaccessible porosity, and it has only the accessible porosity. Next, these tunnels and their ends should be identified. As pointed out before, this is not an obvious task. We have devised a procedure based on sound morphological principals for this purpose. But, let us first explore some simple examples in the plane in order to illustrate our procedure. Let us consider a square with one tunnel in it with trumpet-like ends (Fig. 4A). One way to go is considering the convex hull (Fig. 4B) of the object. In this case the convex hull is a solid square. Then, the accessible porosity is obtained by subtracting the original object from the convex hull (Fig. 4C). As stated above, the convex hull is obtained as the limit set of the process that consists in applying successive morphological closings to the object K. In this way, a series of objects is obtained. The limit of this series is the convex hull (Serra, 1982). A more realistic procedure from a conceptual and computational point of view would be to stop the process when it provides an object with no accessible porosity in it (Fig. 4D), an object which is "solid" and then, it has Euler number equal to one. This method has the advantage of producing an object which volume could be seeing as the volume of the aggregate: it is the minimum object that contains the aggregate and its porosity and, therefore, it is "solid" and it has only one connected component. Also, this procedure provides a more convenient object that can be called a tunnel (Fig. 4E).

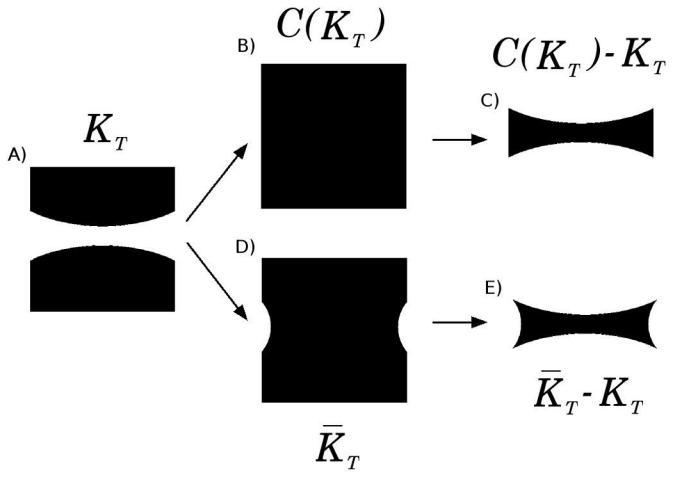

Fig. 4. Geometrical definition of tunnels in the plane: (left) square with a tunnel in it, (upper center) the convex hull of the square with a tunnel in it, (lower center) morphological closure, (upper right) tunnel from the convex hull, and (lower right) tunnel from the morphological closure.

Eventually, the original object has small cracks or hollows that will be smoothed out by the morphological closings. Then, subtracting the original object from the convex hull will yield not only tunnels but also cracks. As a consequence, cracks should be removed after subtraction to stay only with the tunnels. In order to do so, tunnels and cracks will be labeled and added to the original object one at a time. When the new object, which is made up of the original object K and one of the cracks or one of the tunnels, has the same Euler number with the original one, the set added will be a crack and it will be a tunnel when the Euler number varies (Fig. 5). Technical details of the procedure outlined above are left to Appendix B.

4. Results and discussion

4.1. Analyzing aggregate geometry with morphological functions

Fig. 6A and B display the evolution of the volume of the solid part of the aggregates as a function of the diameter of the dilation. As stated above, dilations produce an increase of the volume and this effect is more pronounced when there are tunnels and cavities because dilations reduce them. Dilations turn some voxels with value 0 into voxels with value 1. Roughly speaking, they turn some voxels of the pore space and the exterior of the aggregate into voxels of its solid part. Hence, this morphological operation expands the solid part of the aggregate. Similar relationships between the aggregate volume and dilation radius have been reported by Wang et al. (2012). Fig. 6A indicates that the solid parts of NS aggregates are larger than TM aggregates as values of this function at 0 (i.e. when dilation is performed) are higher for NS aggregates than for TM aggregates. As we will see later, this difference is statistically significant. Fig. 6B shows the evolution of the ratio of the volume of the material of the aggregate to its initial value at 0. It suggests that these relative numbers increase faster for TM aggregates as radius increases. Moreover, the change of the trend for balls of radius three that can be observed in Fig. 6B suggests that most of the porosity should go to a characteristic size of three or less units. Fig. 6A and B shows that more porosity with a characteristic size of three or less units has disappeared as compared with the porosity that disappeared with dilations of characteristic size greater than three units. As this change of trend is more pronounced for TM aggregates than for NS ones, it seems to suggest that TM aggregates should have more voids smaller than this characteristic size as compared with NS aggregates.

Fig. 6C and D displays the evolution of the boundary surface of the aggregate solid part. Loss of aggregate porosity due to dilations decreases soil aggregate boundary surface. As can be seen from the values of this function when r is zero (Fig. 6C), in general, TM aggregates have greater surface area than NS aggregates. The small values of the boundary surface of some TM aggregates should be related to a smoother boundary surface. The decrease of surface is very pronounced till size three, and this decrease is steeper for TM aggregates, also in relative terms (Fig. 6D). This is consistent with the observation relative to volume (Fig. 6A and B). The loss of porosity produces an increase in volume and a decrease in surface. In relative terms (see Fig. 6B and D) as the diameter of dilation grows, TM aggregates get more volume and less surface than NS aggregates. If we assume that the growth of volume and the loss of boundary surface are produced by the reduction of the pore volume, then, the previous observation suggests that TM aggregates should have more porosity (relative volume of tunnels and cavities) than NS aggregates. This observation is consistent with our findings shown below on the aggregate pore space.

The evolution of surface integral of mean curvature and relative surface integral of mean curvature of aggregates are shown in Fig. 6E and F; for brevity we will refer to these two terms as curvature and relative curvature, respectively. The surface boundary of the solid part of aggregates can be thought as made up of two parts; one part is the exterior surface of the aggregate (i.e. the interface with other aggregates and with inter-aggregate porosity) and, the other part is the interior part (i.e. the interface of the solid materials and the pore space of the aggregate). Roughly speaking, while the exterior part of the boundary of

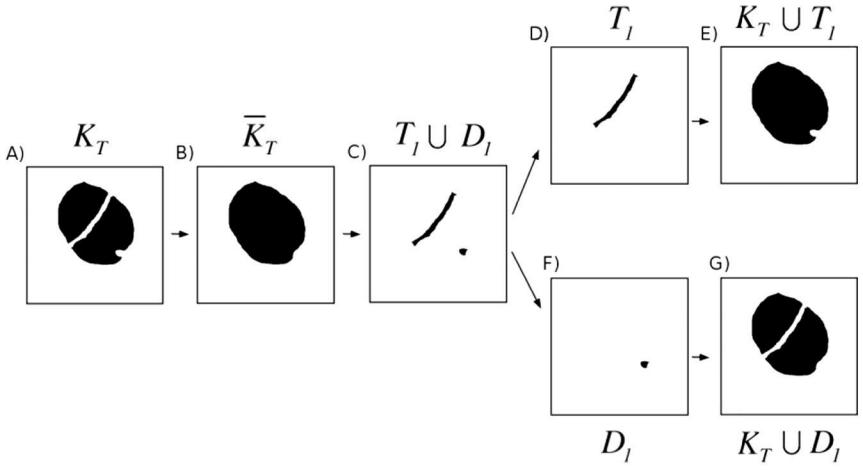

Fig. 5. Distinguishing between tunnels and cracks in the plane: (A) an object with one tunnel and one crack, (B) morphological closure, (C) tunnel plus crack, (D) tunnel, (F) crack, (E) the original object plus the tunnel, and (G) the original object plus the crack.

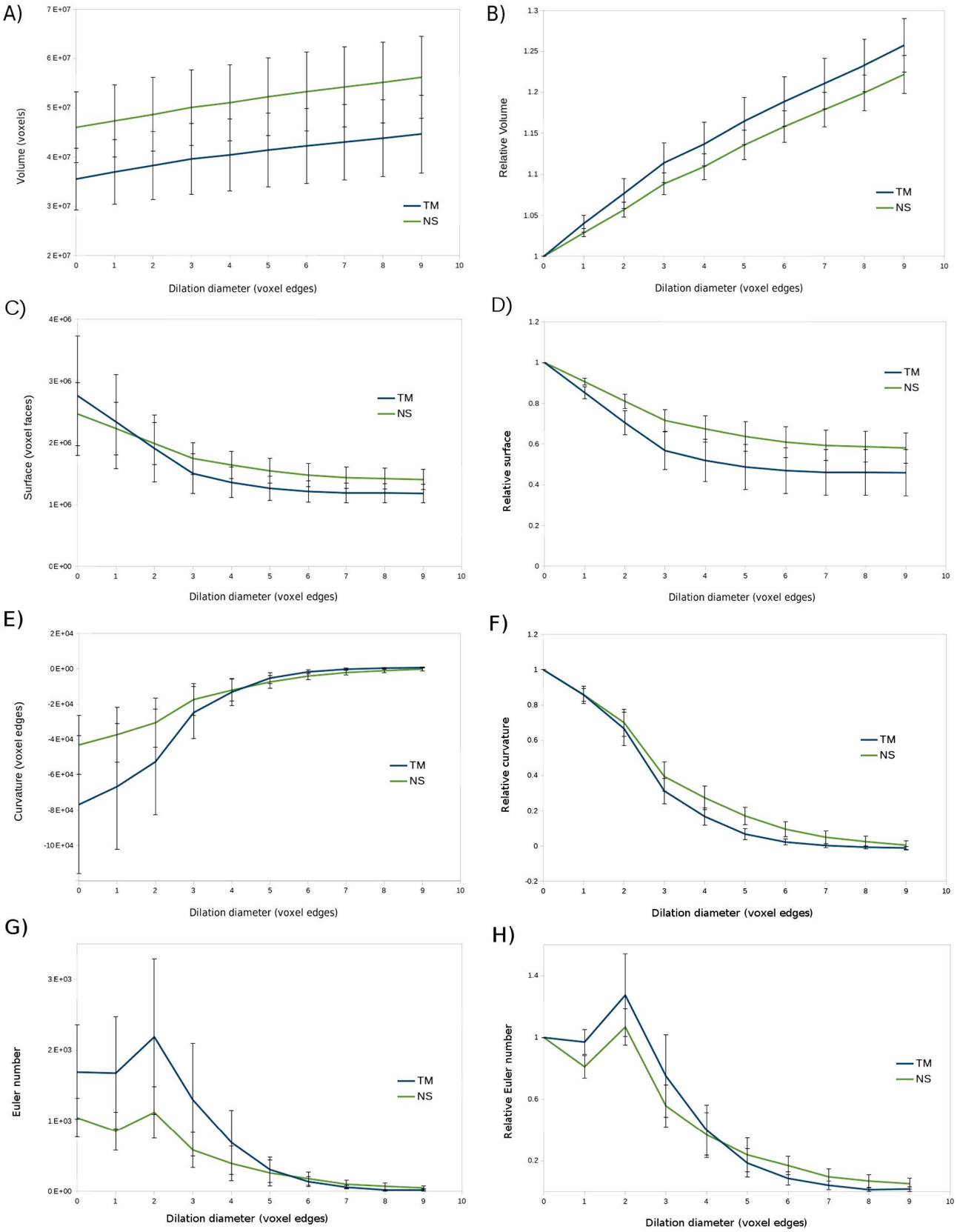

Fig. 6. Evolution of Minkowski functionals for TM and NS aggregates as the radius of the ball used for the dilation grows: A) volume, B) relative volume, C) boundary surface, D) relative boundary surface, E) mean curvatures, F) relative mean curvatures, G) Euler–Poincaré characteristic and H) relative Euler–Poincaré characteristic.

aggregates is convex and should provide positive curvature, the interior is generally concave and should have negative curvature. Therefore, negative values of the curvature of Fig. 6F suggest that most of the total aggregate surface should go to material/void interface. As the diameter of the ball of the dilation grows, cavities and tunnels are thinned or deleted and the boundaries are smoothed out so that the curvature

grows and, in this case, approaches zero. This phenomenon is more accelerated in absolute and relative terms for TM aggregates as shown in Fig. 6E and F. These findings are consistent with our previous comments on the aggregate volumes and surfaces (Fig. 6A, B, C and D).

As the solid part of an aggregate K has only one connected component, i.e. $CC(K) = 1$, the Euler–Poincaré characteristic can be equated to number of cavities, $C(K)$, minus the number of tunnels, $T(K)$, plus one

$$\chi(K) = 1 + C(K) - T(K). \tag{6}$$

Let us note here that as a consequence of this expression, Euler number expresses not only the connectivity of the aggregate but also its porosity in terms of number of tunnels and cavities. Fig. 6G and H shows the change of Euler number (Fig. 6G) and the change of the relative Euler number (Fig. 6H) with the diameter of dilation. All aggregates have positive Euler numbers. This indicates that all aggregates have a bigger amount of cavities than of tunnels. In general, the Euler number is greater for TM aggregates than for NS aggregates. This suggests that the difference between the number of cavities and the number of tunnels is more pronounced in TM aggregates than in NS aggregates. Let us remark that the increase in the Euler number with the diameter of the dilations, that erases cavities and tunnels, could be produced by a higher rate of decrease of the number of tunnels as compared with rate of decrease of the number of cavities. Eventually, dilations will produce new cavities from tunnels when closing narrow passes in tunnels. Therefore, after tunnels have been erased the Euler number begins to fall down as of cavities disappeared by dilations of increasing diameter. Graphs in Fig. 6G and H show a distinct behavior of TM aggregates as compared with NS aggregates. In general, Euler number of TM aggregates grows faster than NS aggregates till size two. This indicates that a great amount of thin tunnels of TM aggregates with narrow passes of size smaller than two units will be closed and transformed into cavities with dilations. NS aggregates instead have a large amount of cavities of characteristic size of one unit as it suggests the decrease of the relative Euler number; this is due to the fact that a decrease of the Euler number should be related to the vanishing of cavities. These graphs also indicate that NS aggregates have a great amount of tunnels with narrow passes of characteristic size equal to two units but to a lesser extent than in the case of TM aggregates. Let us note that the decrease observed in these graphs slows down for values greater than three units. This observation is consistent with the distinct behavior that can be observed at this value in the evolution of volume, surface and curvature (Fig. 6A, B, C, D, E and F). Relative Euler numbers of TM aggregates stabilize for diameters greater than six units and are lower than the values of NS aggregates. This suggests that TM aggregates do not have cavities bigger than balls with diameter six while this type of objects can be found in the interior of NS aggregates. This is coherent with the behavior that is displayed on the graphs of relative volume (Fig. 6A), surface (Fig. 6C) and curvature (Fig. 6E). Visual examination of the aggregate images indeed indicates the presence of large pores of likely biological origin inside many of the NS aggregates. However, such pores hardly ever were observed in the TM aggregates.

Let us summarize the findings of the first part of our analysis. These results suggest that the volume of the solid part of the aggregates with conventional tillage (TM aggregates) is smaller but they have more porosity than the aggregates from soils with natural vegetation succession (NS aggregates). Moreover, there is a great amount of porosity with characteristic size less than three units as it seems to show the change of the evolution of volume, surface, curvature and Euler number of the solid part of aggregates. Euler functions suggest that the porosity of aggregates of soils with conventional tillage (TM aggregates) seems to have a big amount of thin tunnels while aggregates of soils with natural vegetation (NS aggregates) seem to have a bigger amount of small and big cavities. These observations are consistent with the results of Kravchenko et al. (2011) and Wang et al. (2012), who found that TM aggregates are intersected by a connected network of medium sized crack-like pores. Statistical analysis of the apparent differences of Minkowski functionals between aggregates of the two treatments, visible to the naked eye, shows that they were statistically significant except in the case of the surface of the solid part of the aggregates.

4.2. Partition of pore space into accessible and inaccessible porosity

The pore space of aggregates is now considered as the geometric object of interest. Fig. 7 displays values of specific Minkowski functionals of aggregate pore space split between tunnels and cavities. Specific Minkowski functionals are densities. They are defined as the value of the corresponding functional (i.e. volume, surface, curvature and Euler number) relative to the total volume of the aggregate (i.e., the volume of the solid part plus the volume of inner pore space). The apparent visual differences that these graphs seem to suggest have a statistical significance at 5% for all specific geometrical attributes of cavities except for their specific volume. These differences are consistent with our previous findings. In particular, TM aggregates are more porous than NS aggregates and most of these differences in porosity seem to come from tunnels.

When aggregate tunnels or cavities are the object of interest, K, their Euler numbers equate to the number of connected components, $CC(K)$, minus the number of "tunnels" of solid materials through aggregate tunnels or cavities, $T(K)$,

$$\chi(K) = CC(K) - T(K). \tag{7}$$

This is because there is no solid part completely surrounded by voids inside an aggregate tunnel or cavity. Moreover, the specific Euler number of tunnels and cavities (Fig. 7D) and specific number of tunnels and cavities (Fig. 8) are very similar for cavities and very disparate for tunnels. It seems to indicate that in general, the cavities have almost no intrusions of solid materials that completely cross them like "tunnels of solid materials". Therefore, inaccessible porosity is made up of very simple geometrical objects as compared with accessible porosity. In the case of tunnels the difference is obvious to the naked eye. The specific number of tunnels is very small as compared with the specific number of cavities (Fig. 8). Consequently, tunnels display a complex structure as it seems to indicate the negative values of the specific Euler number (Fig. 7D). This seems to suggest that the tunnels of these aggregates should have a big amount of intrusions of solid material through them, i.e. they display a complex and ramified or network-like structure. But it is remarkable that differences between geometrical attributes of tunnels of both samples have no statistical significance.

In order to characterize pore size distribution of aggregates, the equivalent cylindrical diameter (Perret et al., 1999) is considered. Figs. 9 and 10 display the distribution of specific Minkowski functionals by tunnel and cavity sizes, respectively. Six size classes with average sizes of 0.01, 0.02, 0.03, 0.04, 0.05 and 0.06 mm were used. Tunnels were smaller in TM aggregates as compared to NS ones, as the class of tunnels between 0.01 and 0.02 predominates in TM aggregates while the class between 0.02 and 0.03 were the most populated in NS aggregates. Moreover, the difference has a level of statistical significance of 5% in all classes with size less than 0.03. The distribution of cavities by size (Fig. 10) seems to indicate that small cavities of size smaller than 0.02 mm are more abundant in TM aggregates consistent with our analysis of Minkowski functions. In this case, differences between all size classes of cavities of TM and NS aggregates were statistically significant.

We summarize the main findings of our analysis in the following points: (i) differences found between geometrical attributes that convey Minkowski functionals of two treatments were statistically significant in most cases, (ii) TM aggregates were smaller and more porous than NS aggregates, (iii) accessible porosity is made up of geometrical entities with a complex and ramified or network like structure, (iv) inaccessible porosity is composed of mostly simple geometrical objects that generally did not present intrusions of solid material that cross all

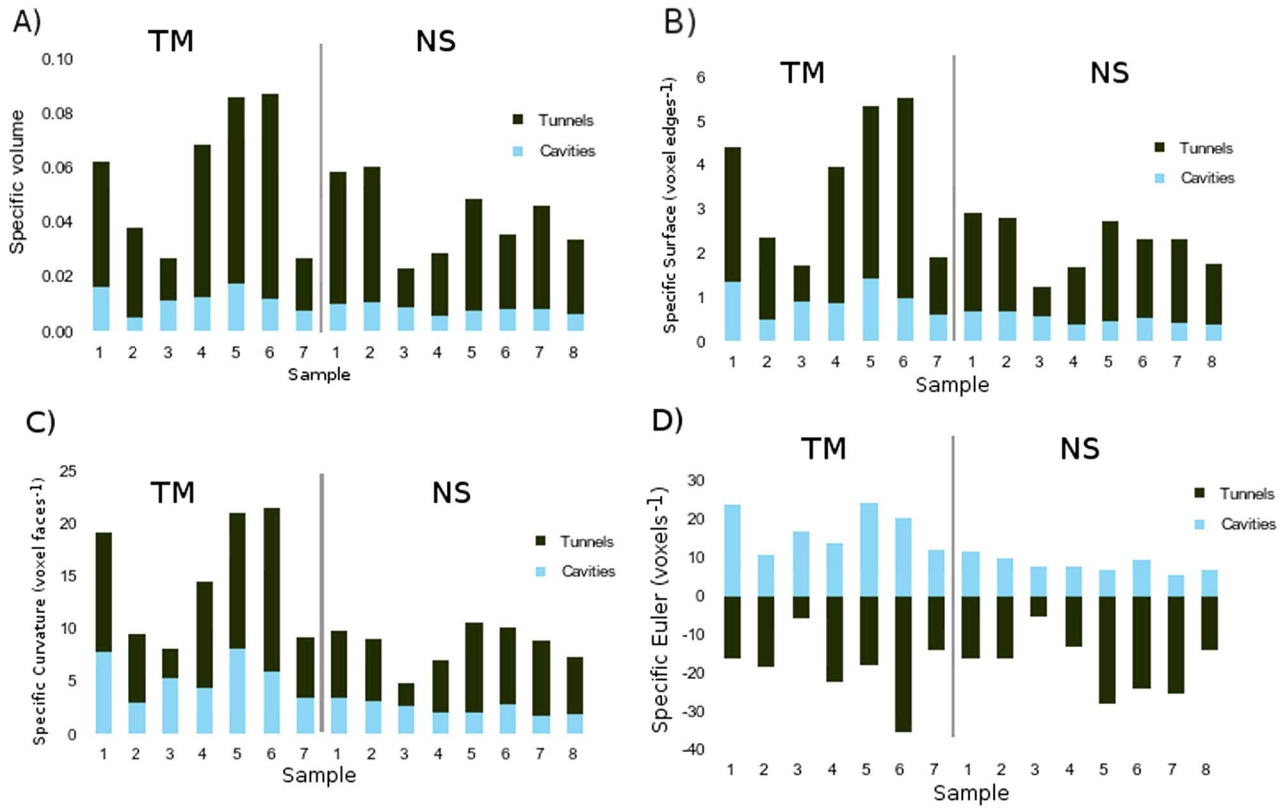

Fig. 7. Specific Minkowski functionals: A), volume, B) surface, C) curvature and D) Euler characteristic, of tunnels and cavities for all TM and NS samples.

over like "tunnels" of slid material through them, (v) thin tunnels seem to populate TM aggregates while the more abundant class of tunnels in NS aggregates had a bigger size, (vi) cavities are more important in number in NS aggregates than in TM ones but small sizes are more frequent in TM aggregates and large size classes are more frequent in NS aggregates, and (vii) geometric attributes of tunnels did not show statistically significant differences between treatments but the differences of the geometrical attributes of cavities were statistically significant. In terms of accessible and inaccessible porosity our results suggest that most of the porosity corresponds to accessible porosity that displayed a complex ramified structure. Small size classes of accessible porosity were abundant in aggregates from soil with conventional tillage (TM aggregates) while larger classes were more abundant in aggregates from soil with natural vegetation (NS aggregates). Inaccessible porosity was a key factor as its geometrical differences discriminate both treatments. Aggregates are regarded as one of the main providers of physical protection of soil organic matter and C sequestration by soils (Six et al., 1999, 2000). One of the mechanisms of such protection is a reduced access of organic material inside the aggregates to decomposing microorganisms. The differences that we are observing in the patterns of accessible and inaccessible porosity between TM and NS aggregates hint at their potentially different effectiveness for protecting C. Clearly, TM aggregates with their network of tunnels will be offering greater microbial access, thus having poorer protection of soil organic matter and C to decomposing microorganisms than the NS aggregates. Observations of Ananyeva et al. (2013) who reported negative relationships between intra-aggregate C and the presence of medium sized intra-aggregate pores support this hypothesis.

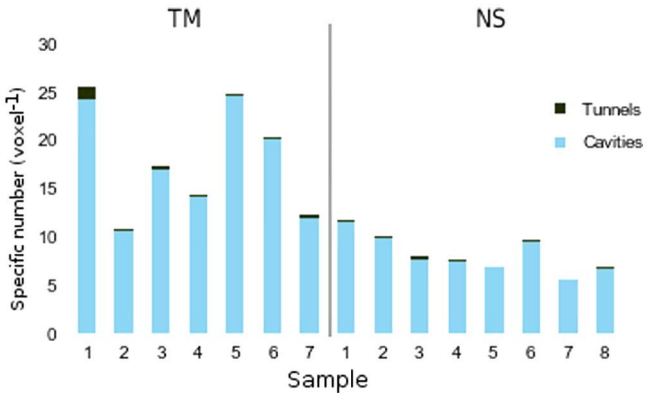

Fig. 8. Specific number of tunnels and cavities for all TM and NS samples.

5. Conclusions

In this work we have introduced the essential tools of mathematical morphology in order to quantify the geometrical morphology of soil aggregates. We made use of 3D images from X-ray CT of aggregates. Aggregates were collected from two different land uses, i.e. conventional tillage management (TM) and native succession vegetation treatment (NS). The ability of morphological tools to capture the impact of soil management on the morphology of these aggregates was explored.

We have presented the building blocks of mathematical morphology, the morphological operations of dilation, erosion, opening and closing and, then, we have dealt with the Minkowski functionals and the Minkowski functions that take account of the evolution of the Minkowski functionals as morphological operations are performed on the 3D object of interest. First, we have considered the solid part of the aggregate as the 3D object of interest and we have investigated the evolution the four Minkowski functionals (i.e. volume, boundary surface, curvature and connectivity) as successive dilations with balls of increasing diameter were performed. That is to say, we have studied the patterns of Minkowski functions building over dilations of the solid part of NS aggregates and TM aggregates. Finally, the inner pore space of aggregates was considered as the object of interest. We have devised a

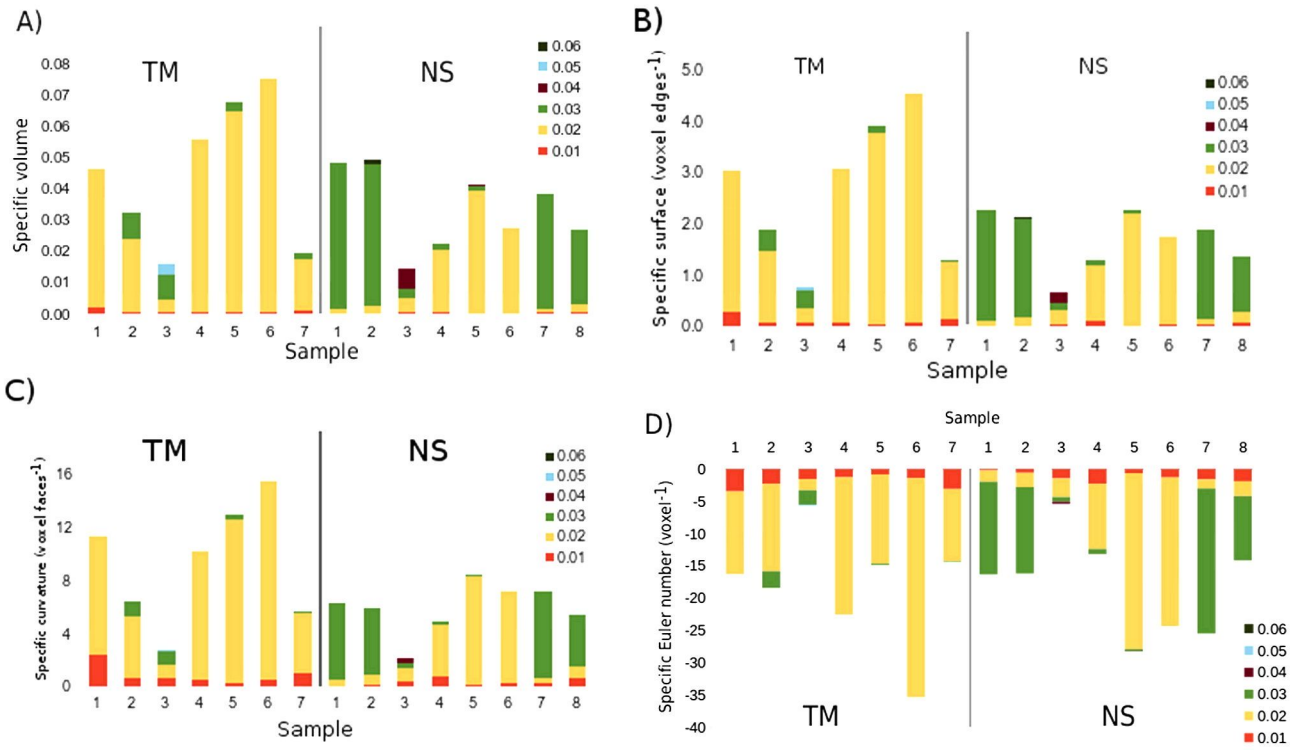

Fig. 9. Distributions of specific Minkowski functionals of tunnels on six pore-size classes for all TM and NS samples: A), volume, B) surface, C) curvature and D) Euler characteristic.

procedure to define the ends of the accessible porosity of the aggregate and to separate aggregate pore space into accessible and inaccessible porosity. In this way, the geometrical attributes of intra-aggregate pore space through their Minkowski functionals provided a complete characterization of the inner aggregate structure. Specifically, we may summarize the observed variation in aggregate structure between the two soil treatments in the following points: (i) TM aggregates were smaller and more porous than NS aggregates, (ii) accessible porosity is made up of geometrical entities with a complex network-like structure, while inaccessible porosity is composed of mostly simple geometrical shapes, (iii) thin tunnels seem to populate TM aggregates while the more abundant class of tunnels in NS aggregates

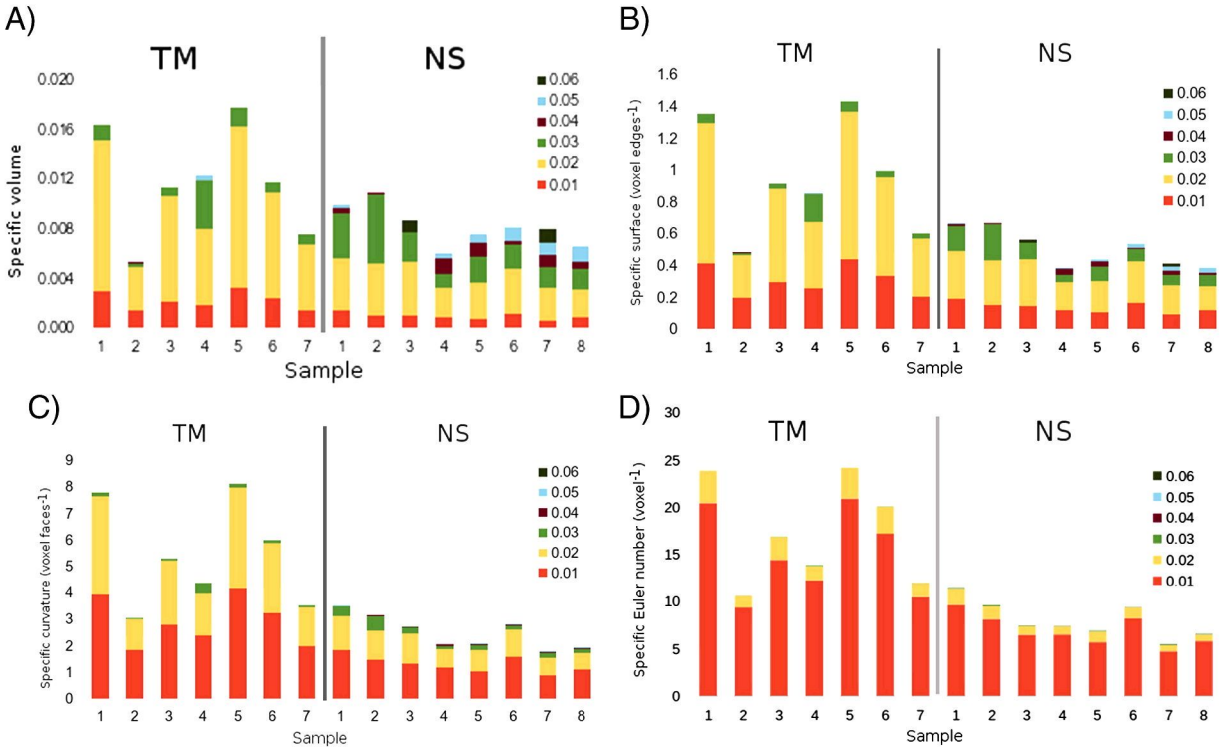

Fig. 10. Distributions of specific Minkowski functionals of cavities on six pore-size classes for all TM and NS samples: A), volume, B) surface, C) curvature and D) Euler characteristic.

had a bigger size, (iv) cavities are more important in number in NS aggregates than in TM ones but small sizes are more frequent in TM aggregates and large size classes are more frequent in NS aggregates, and (v) geometric attributes of tunnels did not show statistically significant differences between treatments but the differences of the geometrical attributes of cavities were statistically significant.

These mathematical techniques have provided an exhaustive quantitative description of soil aggregate morphology of 3D CT images that include both, intra-aggregate pore space structure and aggregate surface features. This morphological description has shown how two different soil treatments affect aggregate structure. Our findings suggest that mathematical morphology is a promising framework to investigate, quantify and characterize soil structure.

Acknowledgments

This work was partially supported by Plan Nacional de Investigación Científica, Desarrollo e Investigación Tecnológica (I + D + i) under ref. AGL2011/251675 and DGUI (Comunidad de Madrid) and UPM under ref. QM100245066.

Appendix A. Morphological analysis

A.1. Morphological operations

Mathematically objects are closed and bounded sets. A ball is a closed set if this ball contains the points of the sphere that defines the ball, its boundary. And, it is a bounded set when it is contained in a sphere of finite radius. Dilation of an object expands it. This new object can be thinking of as the set of points of the union of all balls of a certain size r centered at points of the original object. If the original object is a ball of radius r_0 the dilated object by balls of radius r will be a new ball of radius $r_o + r$. Then, we consider an object K and a ball B of radius one which is centered at the origin of coordinates. Both, K and B, are objects, closed and bounded sets, but K is the object of interest that we scrutinize with the object B that is called structuring element.

A ball of radius r centered at the origin, rB, is obtained by multiplying the points of B by r. A ball of radius one centered at point x, B_x, is obtained by adding x to every point of B. Scalar multiplication by a number r produces an expansion with scaling factor r when $r > 1$, and a contraction with scaling factor r when $r < 1$. Addition with a vector x produces a translation in the direction of the vector x at a distance equal to the "length" of this vector, its modulus. Then, we have the following mathematical expressions that define the sets rB and B_x:

$$rB = \{ry : y \in B\} \text{ and } B_x = \{y + x : y \in B\}. \tag{A.1}$$

That is to say, rB is the set of points ry when y belongs to B and, B_x is the set of points $x + y$ when y belongs to B. In these expressions ry stands for the scalar multiplication of the scalar r and the vector y while $y + x$ represents the sum of two vectors, y and x. Thus, the dilation of the object K by balls of radius r will be another object K_r defined as

$$K_r = \cup_{x \in K} rB_x. \tag{A.2}$$

In others words, the dilated object K_r is the union of all balls rB_x of radius r centered at point x of K. In general, the structuring element could be any set that may or may not contain the origin of coordinates. Then one has $\delta_E(K)$ the dilated set of the object K by structuring element E (Fig. 2). In most cases it is more appropriate to consider structuring elements which contain the origin of coordinates and are symmetric with respect to it: like balls or disks centered at the origin. In this case it is verified that

$$K_r = \delta_{rB}(K). \tag{A.3}$$

The set K_r is called the parallel body of K at a distance r or r-parallel body to K. This is the set of all points within a distance smaller than r from the object K. As we consider balls centered at the origin of coordinates as structuring elements, the dilation of an object by a ball of radius K is equivalent to the r-parallel body to K. Roughly speaking it is like a layer of thickness r is added to K.

In this work two-colored images (black and white images) or binary images correspond to two complementary soil phases: the phase of voids (pore space) and the phase of soil matrix (mineral particles). Then, the erosion of one phase is equivalent to the dilation of the complementary phase. Erosion of the pore space is dilation of the soil matrix and erosion of the soil matrix is dilation of pore space. Usually, a three-dimensional picture of a CT image of soil will be represented by the set of points of a cube S where each point is part of pore space P or is part of soil matrix M. In mathematical terms one has the following expressions

$$S = P \cup M, P^c = M \text{ and } M^c = P. \tag{A.4}$$

Here P^c represents the complementary of P. That expresses the previous statement that the complementary set of the pore space in the cube S is the soil matrix and vice versa. Then, the erosion of an object K by a ball of radius r centered at the origin is defined as

$$\varepsilon_{rB}(K) = \left(\delta_{rB}\left(K^c\right)\right)^c. \tag{A.5}$$

A more intuitive expression is given by

$$\varepsilon_{rB}(K) = \{x : rB_x \subset K\}. \tag{A.6}$$

Consequently, the erosion of an object K by a ball rB corresponds to the set of all positions within K where the structuring element rB fits completely into K (Fig. 3). As a consequence, it is like a layer of thickness r is removed from K.

These morphological operations though complementary in the sense established above do not allow recovering the original object, because neither the dilated set of an eroded one is the original set nor the eroded set of a dilated one is the original set. When dilation is performed after erosion the new morphological operation is an opening:

$$O_{rB}(K) = \delta_{rB}(\varepsilon_{rB}(K)). \tag{A.7}$$

When erosion is performed after dilation the new morphological operation is a closing:

$$C_{rB}(K) = \varepsilon_{rB}(\delta_{rB}(K)). \tag{A.8}$$

Opening and closing are complementary operations of each other as erosions and dilations are

$$C_{rB}(K) = \left(O_{rB}\left(K^c\right)\right)^c \text{ and } O_{rB}(K) = \left(C_{rB}\left(K^c\right)^c\right). \tag{A.9}$$

A.2. Measurements: Steiner formulae and Minkowski functionals

What is the area of a two-dimensional object or the volume of a three-dimensional one when the object is dilated? Let us consider a simple object like a square or a cube with edges of size a and a disk or a ball of radius r as structuring element. In the plane, the area of the dilated object K_r of a square K by a disk rB can easily be computed as

$$A(K_r) = A(\delta_{rB}(K)) = a^2 + 4ar + \pi r^2 = A(K) + L(K)r + A(B)r^2. \tag{A.10}$$

In this expression A stands for the area and L stands for the length of the perimeter of the square K. Here B is the disk centered at the origin with radius one. In 3D space, it is verified that

$$V(K_r) = V(\delta_{rB}(K)) = a^3 + 6a^2 r + 3\pi a r^2 + \frac{4}{3}\pi r^3 = \\ = V(K) + S(K)r + M(K)r^2 + V(B)r^3. \quad (A.11)$$

Here, V stands for the volume, S for the area of the boundary and M for the mean breadth multiplied by 2π (it can be shown that the mean breadth of a cube of edge a is $3a/2$ (Santaló, 1976)). Here B is the ball centered at the origin with radius one.

Now, let us consider a general convex object in d-dimensional linear space, then one has the Steiner formula (Osher and Mücklich, 2000)

$$V(K_r) = \sum_{i=0}^{d} \binom{d}{i} W_i^{(d)}(K). \quad (A.12)$$

In this expression $W_i^{(d)}(K)$ are the Minkowski functionals. There are $d+1$ functionals in dimension d. There are $d+1$ Minkowski functionals in dimension d, $W_i^{(d)}(K)$.

There are three Minkowski functionals in the plane and four in the space, $W_i^{(d)}$ for $d = 2, 3$ and $i = 0, 1, \ldots d$. They are functionals because they are functions that assign a number to any object. For 2D objects in the plane one has

$$W_0^{(2)}(K) = A(K), W_1^{(2)}(K) = L(K) \text{ and } W_2^{(2)}(K) = \pi\chi(K). \quad (A.13)$$

In this expression A stands for the area and L stands for the length of the perimeter of the square K. Here $\chi(K)$ stands for the Euler–Poincaré characteristic of K that is related with the connectivity of the object. For 3D objects in the space one has

$$W_0^{(3)}(K) = V(K), W_1^{(3)}(K) = (1/3)S(K), W_2^{(3)}(K) \\ = (1/3)M(K) \text{ and } W_3^{(3)}(K) = (4\pi/3)\chi(K). \quad (A.14)$$

The first and second Minkowski functionals have simple geometrical interpretations when referring to three dimensional objects in space. They correspond to volume, $V(K)$, and boundary surface area, $S(K)$, respectively. When the boundary surface of a three-dimensional object is smooth the third functional, the surface integral of the mean curvature, $M(K)$, may be interpreted as the mean breadth of the object (Osher and Mücklich, 2000). The last Minkowski functional $W_d^{(d)}$ is the Euler–Poincaré characteristic, $\chi(K)$, of the object up to a factor; this factor is the volume of the d-dimensional ball of radius one. In the plane one has $W_2^{(2)}(K) = \pi\chi(K)$ and $W_3^{(3)}(K) = (4\pi/3)\chi(K)$ in the space.

Minkowski functionals provide a complete set of geometrical measurements as established by Hadwiger's theorem from 1975 (Santaló, 1976). In simple words this theorem states that any functional or geometrical measurement that assigns a number to any object of interest and fulfills some very natural geometrical restrictions is a linear combination of the Minkowski functionals with numbers as scalars of this linear combination. Let us be more precise and specify which the objects of interest and the geometrical conditions are. On the one hand, a class of objects to which Hadwiger's theorem applies is the class of sets that can be viewed as the union of a finite number of convex objects. This is a very important class of objects because any three-dimensional binary image is a set of voxels (the three-dimensional counterpart of a pixel). These voxels are cubes and then, any geometrical structure of interest in an image is a finite union of convex objects, the voxels. On the other hand, three are the geometrical conditions that must fulfill any functional to which Hadwiger's theorem applies. The first one is motion invariance: the number assigned by a functional must be independent of the position of the object in space when the object is translated or rotated. The second one is C-additivity:

$$\mathscr{F}(K_1 \cup K_2) = \mathscr{F}(K_1) + \mathscr{F}(K_2) - \mathscr{F}(K_1 \cap K_2). \quad (A.15)$$

That is to say: the number assigned by a functional to the union of two objects equals the value of the functionals over those two objects minus parts counted twice. And the third one is continuity. Consider a sequence of objects $\{K_n\}$ that approaches to the object K as n tends to infinity. An example of this, is the sequence of r-parallel bodies of an object K; it is clear that the sequence of r-parallel bodies $\{K_n\}$ with $n = 1/r$, tends to go to K as n goes to infinity or, equivalently, as r goes to zero. Then, the continuity condition is fulfilled if $\mathscr{F}(K_n)$ tends to go to $\mathscr{F}(K)$ as n goes to infinity. Under these conditions there are $d+1$ numbers, c_i, in the d-dimensional linear space such that

$$\mathscr{F}(K) = \sum_{i=0}^{d} c_i W_i^{(d)}(K). \quad (A.16)$$

Appendix B. Partition of aggregate pore space: technical details

Let us summarize the procedure to split aggregate pore space between accessible and inaccessible porosity outlined in Section 3. Let us say that W is the set of voxels of the image and K the set of voxels of the object of interest (i.e. the solid part of the aggregate), then $W = K \cup K^c$ where K^c stands for the complementary of K, as stated above; K^c is the background. Labeling the image will yield the following connected components: the material of the aggregate, K, the set of all the voxels of the accessible porosity and the "exterior" of the aggregate, T and the cavities C_k, for $k = 1, \ldots, p$. Let us note that $K^c = T \cup (\cup_{k=1}^{p} C_k)$. First, object $K_T = K \cup (\cup_{k=1}^{p} C_k)$ is obtained. This new object includes the material part of aggregate K and their cavities. Then, K_T has only accessible porosity. Second, the new object $\overline{K}_T$, that contains the material and the porosity of the aggregates, is generated. In order to do so, $C_{rB}(K_T)$ is produced by successive morphological closings with balls of increasing radius r performed on the object K_T till it reached the value s that verifies $\chi(C_{rB}(K_T)) = 1$ for $r \geq s$. That is to say, $C_{sB}(K_T)$ has only one connected component, i.e. it is "solid" without any void in it (i.e. without porosity). Then, $\overline{K}_T = C_{sB}(K_T)$. Third, we produce the set of tunnels as follows. By the intersection $\overline{K}_T \cap {K_T}^c$, the tunnels T_i and the cracks (depressions or craters of the surface of the aggregates) D_j will be obtained. Therefore, $\overline{K}_T \cap {K_T}^c = (\cup_{i=1}^{n} T_i) \cup \left(\cup_{j=1}^{m} D_j\right)$. Tunnels will be distinguished from the cracks or depressions of the surface of the aggregate taking into account that $\chi(K_T \cup T_i) = \chi(K_T) + 1$ and $\chi(K_T \cup D_i) = \chi(K_T)$. Then, objects T_i, for $i = 1 \ldots n$, the tunnels of the aggregates and objects C_k, for $k = 1, \ldots, p$, the cavities, are identified. Hence, $P = (\cup_{i=1}^{n} T_i) \cup (\cup_{k=1}^{p} C_k)$ will be the porosity of the aggregate, $(\cup_{i=1}^{n} T_i)$ will be the accessible porosity and $(\cup_{k=1}^{p} C_k)$ the inaccessible porosity.

References

Ananyeva, K., Wang, W., Smucker, A.J.M., Rivers, M.L., Kravchenko, A.N., 2013. Intra-aggregate pore structures are related to total C distribution within soil macroaggregates. Soil Biol. Biochem. 57, 868–875.

Arns, C.H., Knackstedt, M.A., Mecke, K.R., 2002. Characterizing the morphology of disordered materials. In: Mecke, K.R., Stoyan, D. (Eds.), Morphology of Condensed Matter. LNP 600. Springer-Verlag, Berlin, Germany, pp. 37–74.

Arns, C.H., Knackstedt, M.A., Mecke, K.R., 2004. Characterisation of irregular spatial structures by parallel sets and integral geometric measures. Colloids Surf. A Physicochem. Eng. Aspects 241, 351–372.

Banhart, J. (Ed.), 2008. Advanced Tomographic Methods in Materials Research and Engineering. Oxford University Press, Oxford, UK.

Blackwood, C.B., Dell, C.J., Smucker, A.J.M., Paul, E.A., 2006. Eubacterial communities in different soil macroaggregate environments and cropping systems. Soil Biol. Biochem. 38, 720–728.

Chenu, C., Plante, A.F., 2006. Clay-sized organo-mineral complexes in a cultivation chronosequence: revisiting the concept of the primary organo-mineral complex. Eur. J. Soil Sci. 57, 596–607.

Chung Chun, H., Giménez, D., Won Yoon, S., 2008. Morphology, lacunarity and entropy of intra-aggregate pores: aggregate size and soil management effects. Geoderma 146, 83–93.
De Gryze, S., Six, J., Paustian, K., Morris, S.J., Paul, E.A., Merckx, R., 2004. Soil organic carbon pool changes following land-use conversions. Glob. Change Biol. 10, 1120–1132.
De Gryze, S., Jassogne, L., Six, J., Bossuyt, H., Wevers, M., Merckx, M., 2006. Pore structure changes during decomposition of fresh residue: X-ray tomography analyses. Geoderma 134, 82–96.
Dullien, F.A.L., 1992. Porous Media: Fluid Transport and Pore Structure, Second edition. Academic Press, Inc.
Ellerbrock, R.H., Gerke, H.H., 2004. Characterizing organic matter of soil aggregate coatings and biopores by Fourier transform infrared spectroscopy. Eur. J. Soil Sci. 55, 219–228.
Gibson, J.R., Lin, H., Bruns, M.A., 2006. A comparison of fractal analytical methods on 2- and 3-dimensional computed tomographic scans of soil aggregates. Geoderma 134, 335–348.
Giménez, D., Karmon, J.L., Posadas, A., Shaw, R.K., 2002. Fractal dimensions of mass estimated from intact and eroded soil aggregates. Soil Tillage Res. 64, 165–172.
Gonzalez, R.C., Woods, R.E., 2008. Digital Image Processing. Pearson, Prentice Hall, Upper Saddle Rive, New Jersey, USA.
Grandy, A.S., Robertson, G.P., 2007. Land-use intensity effects on soil organic carbon accumulation rates and mechanisms. Ecosystems 10, 58–73.
Horgan, G.W., 1998. Mathematical morphology for analyzing soil structure from images. Eur. J. Soil Sci. 49, 161–173.
Iassonov, P., Gebregenus, T., Tuller, M., 2009. Segmentation of X-ray CT images of porous materials: a crucial step for characterization and quantitative analysis of pore structures. Water Resour. Res. 45, W09415. http://dx.doi.org/10.1029/2009WR008087.
Jasinska, E., Baumgartl, T., Wetzel, H., Horn, R., 2006. Heterogeneity of physico-chemical properties in structured soils and its consequences. Pedosphere 16, 284–296.
Kellogg Biological Station, 2011. Experimental Design. KBS, Hickory Coner, MI [online]. Available at: http://lter.kbs.msu.edu/about/experimental_design.php (accessed 31. 07.11).
Klette, R., Rosenfeld, A., 2004. Digital geometry. Geometric methods for digital picture analysisMorgan Kaufmann Series in Computer Graphics and Geometric Modeling. Morgan Kaufmann, San Francisco, USA.
Kong, T.Y., Rosenfeld, A., 1989. Digital topology: introduction and survey. Comput. Vis. Graph. Image Process. 48, 357–393.
Kravchenko, A.N., Wang, W., Smucker, A.J.M., Rivers, M.L., 2011. Long-term differences in tillage and land use affect intra-aggregate pore heterogeneity. Soil Sci. Soc. Am. J. 75, 1658–1666.
Lehmann, P., 2005. Pore structures: measurement, characterization and relevance for flow and transport in soils. Proc. Appl. Math. Mech. 5, 39–42.
Lehmann, P., Wyss, P., Flisch, A., Lehmann, E., Vontobel, P., Krafczyk, M., Kaestner, A., Beckmann, F., Gygi, A., Flühler, H., 2006. Tomographical imaging and mathematical description of porous media used for the prediction of fluid distribution. Vadose Zone J. 5l, 80–97.
Likos, C.N., Mecke, K.R., Wagner, H., 1995. Statistical morphology of random interfaces in microemulsions. J. Chem. Phys. 102, 9350–9360.
Matheron, G., 1975. Random Sets and Integral Geometry. John Wiley & Sons, Inc., New York, USA.
Mecke, R.K., 1998. Integral geometry in statistical physics. Int. J. Mod. Phys. B 12, 861–899.
Mecke, K.R., 2002. The shape of parallel surfaces: porous media, fluctuating interfaces and complex fluids. Physica A 314, 655–662.
Mecke, K., Arns, C.H., 2005. Fluids in porous media: a morphometric approach. J. Phys. Condens. Matter 17, S503–S534.
Michielsen, K., De Raedt, H., 2001. Integral-geometry morphological image analysis. Phys. Rep. 347, 461–538.
Moran, C.J., McBratney, A.B., Koppi, A.J., 1989a. A rapid method for analysis of soil macropore structure. I. Specimen preparation and digital binary image production. Soil Sci. Soc. Am. J. 53, 921–928.
Moran, C.J., McBratney, A.B., Koppi, A.J., 1989b. A rapid method for analysis of soil macropore structure. II. Stereological model, statistical analysis. And interpretation. Soil Sci. Soc. Am. J. 53, 509–515.
Nunan, N., Ritz, K., Rivers, M., Feeney, D.S., Young, I.M., 2006. Investigating microbial micro-habitat structure using X-ray computed tomography. Geoderma 133, 398–407.
Osher, J., Mücklich, F., 2000. Statistical Analysis of Microstructure in Materials Sciences. John Wiley & Sons, Chichester, England.
Papadopoulos, A., Mooney, S.J., Bird, N.R.A., 2006. Quantification of the effects of contrasting crops in the development of soil structure: an organic conversion. Soil Use Manag. 22, 172–179.
Perret, J., Prasher, S.O., Kantzas, A., Langford, C., 1999. Three-dimensional quantification of macropore networks in undisturbed soil cores. Soil Sci. Soc. Am. J. 63, 1530–1543.
Peth, S., Horn, R., Beckmann, F., Donath, T., Fischer, J., Smucker, A.J.M., 2008. Three-dimensional quantification of intra-aggregate pore-space features using synchrotron-radiation-based microtomography. Soil Sci. Soc. Am. J. 72, 897–907.
Rosenfeld, A., Pfaltz, J.L., 1966. Sequential operations in digital picture processing. J. ACM 13, 471–494.
Roth, R., Boike, J., Vogel, H.J., 2005. Quantifying permafrost patterns using Minkowski densities. Permafr. Periglac. Process. 16, 277–290.
Santaló, L.A., 1976. Integral Geometry and Geometric Probability. Addison-Wesley Publishing Co. Inc., Reading, Massachusetts, USA.
Santos, D., Murphy, S.L.S., Taubner, H., Smucker, A.J.M., Horn, R., 1997. Uniform separation of concentric surface layers from aggregates. Soil Sci. Soc. Am. J. 61, 720–724.
Serra, J., 1982. Image Analysis and Mathematical Morphology. Academic Press Inc., Orlando, Florida, USA.
Sexstone, A.J., Revsbech, N.P., Parkin, T.B., Tiedje, J.M., 1985. Direct measurement of oxygen profiles and denitrification rates in soil aggregates. Soil Sci. Soc. Am. J. 49, 645–651 (1377).
Six, J., Elliott, E.T., Paustian, K., 1999. Aggregate and soil organic matter dynamics under conventional and no-tillage systems. Soil Sci. Soc. Am. J. 63, 1350–1358.
Six, J., Elliott, E.T., Paustian, K., 2000. Soil macroaggregate turnover and microaggregate formation: a mechanism for C sequestration under no-tillage agriculture. Soil Biol. Biochem. 32, 2099–2103.
Soille, P., 2002. Morphological textural analysis: an introduction. In: Mecke, K.R., Stoyan, D. (Eds.), Morphology of Condensed Matter. LNP 600. Springer-Verlag, Berlin, Germany, pp. 215–237.
Sonka, M., Hlavac, V., Boyle, R., 1998. Image Processing, Analysis, and Machine Vision, 2nd ed. PWS, an Imprint of Brooks and Cole Publishing Inc.
Urbanek, E., Hallett, P., Feeney, D., Horn, R., 2007. Water repellency and distribution of hydrophilic and hydrophobic compounds in soil aggregates from different tillage systems. Geoderma 140, 147–155.
Vogel, H.J., 2002. Topological characterization of porous media. In: Mecke, K.R., Stoyan, D. (Eds.), Morphology of Condensed Matter. LNP 600. Springer-Verlag, Berlin, Germany, pp. 75–92.
Vogel, H.J., Kretzschmar, A., 1996. Topological characterization of pore space in soil – sample preparation and digital image-processing. Geoderma 73, 23–38.
Vogel, H.J., Hoffmann, H., Roth, K., 2005. Studies of crack dynamics in clay soil. I. Experimental methods, results, and morphological quantification. Geoderma 125, 203–211.
von Lützow, M., Kögel-Knabner, I., Ekschmitt, K., Matzner, E., Guggenberger, G., Marschner, B., Flessa, H., 2006. Stabilization of organic matter in temperate soils: mechanisms and their relevance under different soil conditions—a review. Eur. J. Soil Sci. 57, 426–445.
Wang, W., Kravchenko, A.N., Smucker, A.J.M., Liang, W., Rivers, M.L., 2012. Intra-aggregate pore characteristics: X-ray computed microtomography analysis. Soil Sci. Soc. Am. J. 76, 1159–1171.
Whalley, W.R., Riseley, B., Leed-Harison, P.B., Bird, N.R.A., Leech, P.K., Adderley, W.P., 2005. Structural differences between bulk and rhizosphere soil. Eur. J. Soil Sci. 56, 353–360.
Young, I.M., Crawford, J.W., 1991. The fractal structure of soil aggregates: its measurement and interpretation. J. Soil Sci. 42, 187–192.
Zhou, H., Peng, X., Perfect, E., Xiao, T., Peng, G., 2013. Effects of organic and inorganic fertilization on soil aggregation in an Ultisol as characterized by synchrotron based X-ray micro-computed tomography. Geoderma 195–196, 23–30.
Zucca, C., Vignozzi, N., Madrau, S., Dingil, M., Previtali, F., Kapur, S., 2013. Shape and intraporosity of topsoil aggregates under maquis and pasture in the Mediterranean región. J. Plant Nutr. Soil Sci. 176, 529–539.